PUBLICATIONS OF THE ASTRONOMICAL SOCIETY OF THE PACIFIC, **123**:263–274, 2011 March

OCam with CCD220, the Fastest and Most Sensitive Camera to Date for AO Wavefront Sensing

PHILIPPE FEAUTRIER,[1] JEAN-LUC GACH,[2] PHILIPPE BALARD,[2] CHRISTIAN GUILLAUME,[3] MARK DOWNING,[4]
NORBERT HUBIN,[4] ERIC STADLER,[1] YVES MAGNARD,[1] MICHAEL SKEGG,[5] MARK ROBBINS,[5]
SANDY DENNEY,[5] WOLFGANG SUSKE,[5] PAUL JORDEN,[5] PATRICK WHEELER,[5]
PETER POOL,[5] RAY BELL,[5] DAVID BURT,[5] IAN DAVIES,[5] JAVIER REYES,[4]
MANFRED MEYER,[4] DIETRICH BAADE,[4] MARKUS KASPER,[4]
ROBIN ARSENAULT,[4] THIERRY FUSCO,[6] AND
JOSÉ JAVIER DIAZ GARCIA[7]

Received 2010 June 24; accepted 2010 December 21; published 2011 February 10

ABSTRACT. For the first time, subelectron readout noise has been achieved with a camera dedicated to astronomical wavefront-sensing applications. The OCam system demonstrated this performance at a 1300 Hz frame rate and with 240×240 pixel frame size. ESO and JRA2 OPTICON jointly funded e2v Technologies to develop a custom CCD for adaptive optics (AO) wavefront-sensing applications. The device, called CCD220, is a compact Peltier-cooled 240×240 pixel frame-transfer eight-output back-illuminated sensor using the EMCCD technology. This article demonstrates, for the first time, subelectron readout noise at frame rates from 25 Hz to 1300 Hz and dark current lower than $0.01\ e^-$ pixel^{-1} frame^{-1}. It reports on the quantitative performance characterization of OCam and the CCD220, including readout noise, dark current, multiplication gain, quantum efficiency, and charge transfer efficiency. OCam includes a low-noise preamplifier stage, a digital board to generate the clocks, and a microcontroller. The data acquisition system includes a user-friendly timer file editor to generate any type of clocking scheme. A second version of OCam, called OCam^2, has been designed to offer enhanced performance, a completely sealed camera package, and an additional Peltier stage to facilitate operation on a telescope or environmentally challenging applications. New features of OCam^2 are presented in this article. This instrumental development will strongly impact the performance of the most advanced AO systems to come.

Online material: color figures

1. INTRODUCTION

The success of the next generation of ESO (European Southern Observatory) instruments (Moorwood 2006) for 8 to 10 m class telescopes will depend on the ability of adaptive optics (AO) systems to provide excellent image quality and stability. This will be achieved by increasing the sampling of the wavefront errors in both spatial and time domains. For example, advanced Shack-Hartmann systems currently fabricated require 40×40 subapertures at sampling rates of 1–1.5 kHz, as opposed to the 14×14 subapertures at 500 Hz of previous AO systems. Detectors of 240×240 pixels are required to provide spatial sampling of 5–6 pixels subaperture^{-1}. Higher temporal-spatial sampling implies fewer photons per pixel and therefore the need for much lower readout noise ($\ll 1\ e^-$) and negligible dark current ($\ll 1\ e^-$ pixel^{-1} frame^{-1}) to perform centroiding computation on a small number of photons.

The detector development described in this article was jointly funded by ESO and the OPTICON (Optical Infrared Coordination Network) European network (Gillmore 2004) in the Joint Research Activity (JRA2; Feautrier et al. 2006), "Fast Detectors for Adaptive Optics." The company e2v Technologies was chosen in 2005 to develop a dedicated detector based on an extension of their L3Vision (Jerram et al. 2001) electron-multiplying charge-coupled-device (EMCCD) technology. Analysis (Fusco et al. 2004) showed that the subelectron readout noise of L3Vision CCDs clearly outperformed classical CCDs, even though

[1] Université Joseph Fourier-Grenoble 1/CNRS-INSU, Institut de Planétologie et d'Astrophysique de Grenoble (IPAG) UMR 5274, Grenoble, F-38041, France; philippe.feautrier@obs.ujf-grenoble.fr.
[2] Laboratoire d'Astrophysique de Marseille (LAM), Technopôle de Château-Gombert-38, rue Frédéric Joliot-Curie, F-13388 Marseille, France.
[3] Observatoire de Haute Provence (OHP), F-04870 St. Michel l'Observatoire, France.
[4] ESO, Karl-Schwarzschild-Strasse 2, D-85748 Garching bei München, Germany.
[5] e2v Technologies, 106 Waterhouse Lane, Chelmsford, Essex, CM1 2QU, England.
[6] ONERA, BP 72, F-92322 Chatillon Cedex, France.
[7] Instituto de Astrofisica de Canarias (IAC), E-38200 La Laguna, Islas Canarias, Spain.

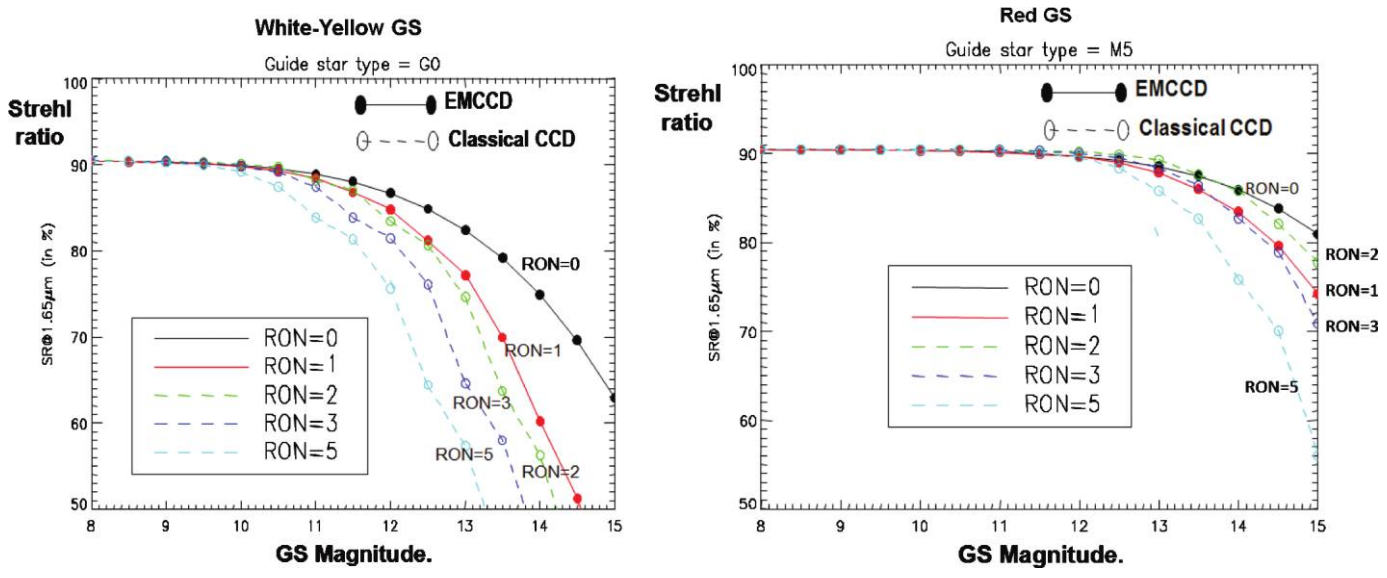

FIG. 1.—Results of analysis performed for the ESO instrument SPHERE (Fusco et al. 2004) that compares an EMCCD of readout noise (RON) 0 and 1 e^- with a classical CCD of readout noise 2, 3, and 5 e^- for two different types of guide stars. *Left*: Plots of Strehl ratio vs. guide-star magnitude for white-yellow types of guide stars. *Right*: Plots of Strehl ratio vs. guide-star magnitude for red types of guide stars.

L3Vision devices exhibit the excess noise factor F of $2^{1/2}$, which is typical of EMCCDs (Robbins & Hadven 2003). The reason for this conclusion is clearly shown in the results (see Fig. 1) of an analysis (Petit et al. 2008) for the ESO instrument SPHERE (Spectro-Polarimetric High-Contrast Exoplanet Research; Beuzit et al. 2008) for two different types of natural guide stars (GSs): white-yellow and red. We observed that a much higher Strehl ratio is achieved for a faint guide star by an EMCCD than by a classical CCD, even though it was assumed that the classical CCD had higher quantum efficiency with red guide stars. Figure 2 illustrates Ocam integration in the SPHERE AO system.

2. THE CCD220 DESIGN

The e2v Technologies CCD220 (Feautrier et al. 2008; Downing et al. 2006, 2006, 2008) (schematic and pinout in

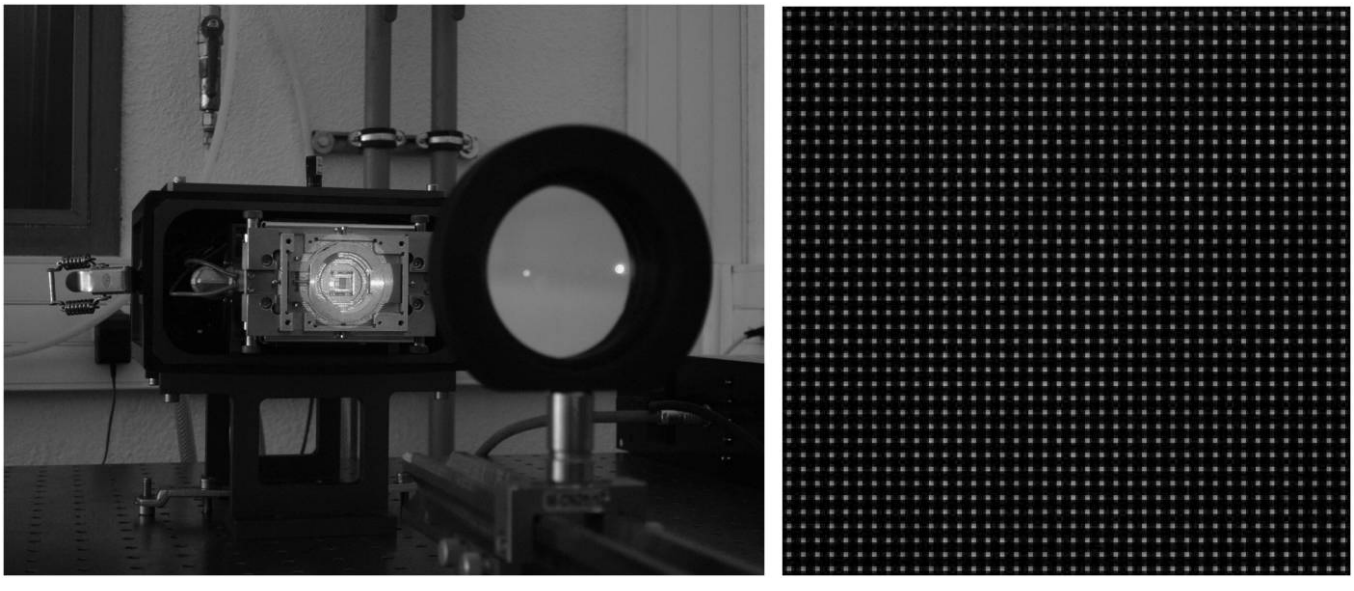

FIG. 2.—40×40 microlens array integration on OCam prototype for SPHERE (Fusco et al. 2004) AO loop testing. *Left*: Test setup for microlens alignment and integration. *Right*: Image of the 40×40 lenslet array on OCam. See the electronic edition of the *PASP* for a color version of this figure.

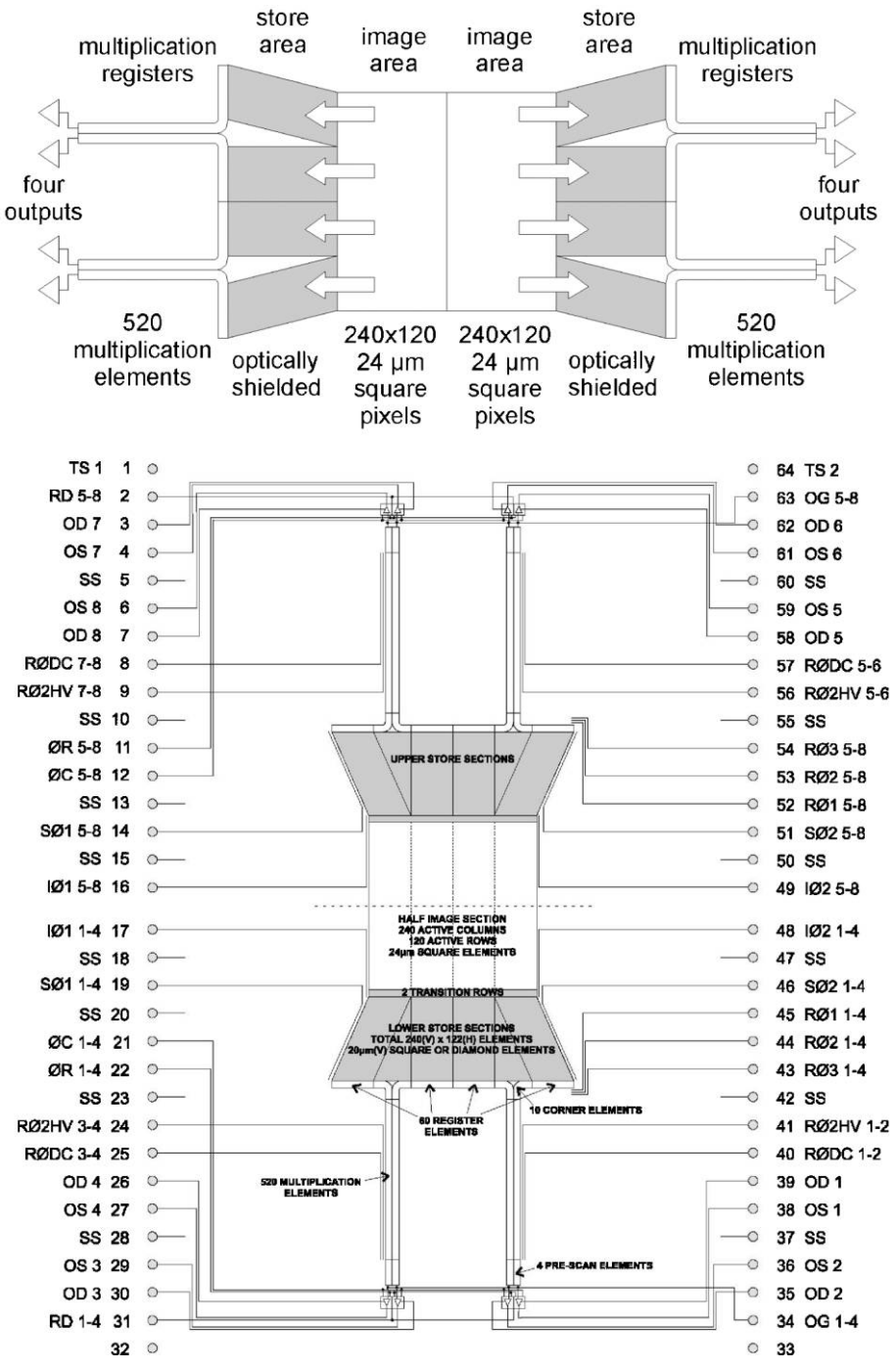

FIG. 3.—*Top*: Schematic of e2v Technologies 240×240 pixel L3Vision CCD220. Eight electron-multiplying (gain) registers are used to obtain subelectron noise at frame rates of 1300 fps. *Bottom*: CCD220 pinout. See the electronic edition of the *PASP* for a color version of this figure.

Fig. 3) is a 24 μm square 240×240 pixel split frame-transfer back-illuminated L3Vision CCD. The image and store area (store is optically shielded) are built with two-phase metal-buttressed parallel clock structures to enable fast line shifts in excess of 7 Mlines s^{-1} for total transfer time from image to store of 18 μs and low smearing of under 2% at 1200 fps. Eight electron-multiplying (Jerram et al. 2001) registers operating at greater than 13 Mpixels s^{-1} enable subelectron noise at frame rates of 1300 fps.

The CCD220 is encapsulated in a 64-pin package (see Fig. 4) with a custom-designed integral Peltier cooler that cools the CCD to below -45°C to achieve the required total dark current.

FIG. 4.—Photograph of CCD220 package with integral Peltier cooler that has been verified (first by thermal modeling, then by measurement) to cool the CCD below -45°C to achieve $<0.01\ e^-$ pixel^{-1} frame^{-1} total dark current. See the electronic edition of the *PASP* for a color version of this figure.

The package is sealed and back-filled with 0.9 bar of krypton gas to minimize heat transfer to the outside. Extensive thermal modeling of the CCD, Peltier cooler, package, proposed clamping arrangement, and water-cooled heat exchanger was performed (Feautrier et al. 2006). The modeling results were verified by measurement and showed that for 10°C water temperature inside the heat exchanger, the Peltier can cool the CCD to below -45°C. This enables the dark current specification ($<0.01\ e^-$ pixel^{-1} frame^{-1} at 1300 fps and $<0.04\ e^-$ pixel^{-1} frame^{-1} at 25 fps) of the standard silicon device to be easily achieved.

3. THE OCAM CONTROLLER

3.1. The OCam Controller Presentation

The OCam camera was designed to test and operate the CCD220. The analog electronics of OCam also forms a critical part of the adaptive-optics branch of ESO's NGC controller (Reyes & Conzelman 2009).

The controller is divided into four parts that are shown in Figure 5: an acquisition system, an interface board, the internal microcontroller that manages the drive electronics, and the link to the data acquisition system controller.

The design was carefully optimized for ultra–low-noise operation. Particular care was taken to minimize radio-frequency perturbations. The drive electronics were designed to be as close as possible to the CCD in order to minimize parasitic inductance (from tracks/pins) and to enable high parallel clocking frequencies (see Fig. 6). With the OCam design, only a few centimeters separate the CCD die from the video preamplifiers.

3.2. Main OCam Controller Characteristics

The OCam system is able to drive the CCD220 at its nominal speed (1500 frames s^{-1}) and to transmit data in real time at this speed through a CameraLink interface. The camera controller is able to drive deep depleted variants with multilevel clocking at voltage levels up to 24 V with speeds of 10 Mlines s^{-1} (at a nominal phase load of 1 nF). For such frame rates, OCam uses a special phase-generation scheme using an arbitrary waveform generator. The core sequencer feeds a fast 14 bit D/A converter running at 109 Mfps, followed by a class AB power amplifier that drives the CCD's phase. Using this generation method, it is possible to compensate for the parasitic printed circuit board track/package pin inductance that makes a resonator with the CCD's phase and to produce potentially destructive overshoots by using deemphasis and suitable drive waveforms. This method can also be used to reduce the slew rate of the phase drive in order to minimize the clock-induced charges (Gach et al. 2006).

The controller handles the eight L3vision outputs with high voltage, clocking up to 50 V voltage swings. Great effort has been made to ensure high-voltage stability (less than 1 mV hr^{-1} of drift) in order to provide a constant gain over a long period. The system digitizes the CCD signal using correlated double sampling with 14 bit resolution. Standard interfacing of the camera is performed by using a PC computer running a Windows operating system with a CameraLink frame grabber and proprietary software. The system is able to acquire, in real time, the 220 Mbytes s^{-1} extremely high data rate produced by the camera.

In addition, the team developed a user-friendly timer file editor to manage the clock sequencer of OCam. The sequencer itself is the heart of the system; it has a nominal resolution of 1.5 ns and is able to generate clocks at a frequency of 327 MHz. The phase jitter was measured at a level of 60 ps rms.

For the detector operating conditions, we used typical pulse amplitudes and DC levels recommended by e2v Technologies; see Figure 3 for the pinout definition of the CCD220. This is listed in Table 1.

4. OCAM AND CCD220 PERFORMANCES

The calibration and performance measurement of OCam and the CCD220 requires nonstandard techniques, due to the extreme performances of this system. The main calibration methods are described in this section, including measured performance.

4.1. System Gain Calibration

Camera calibrations usually rely on the photon-transfer curve, which plots the signal variance as a function of the signal level. At medium signal level, a digital camera is normally shot-noise-limited, as this exceeds the readout noise floor. The shot noise is characterized by the fact that its rms value is equal to the square root of the mean number of incident photons on a given pixel.

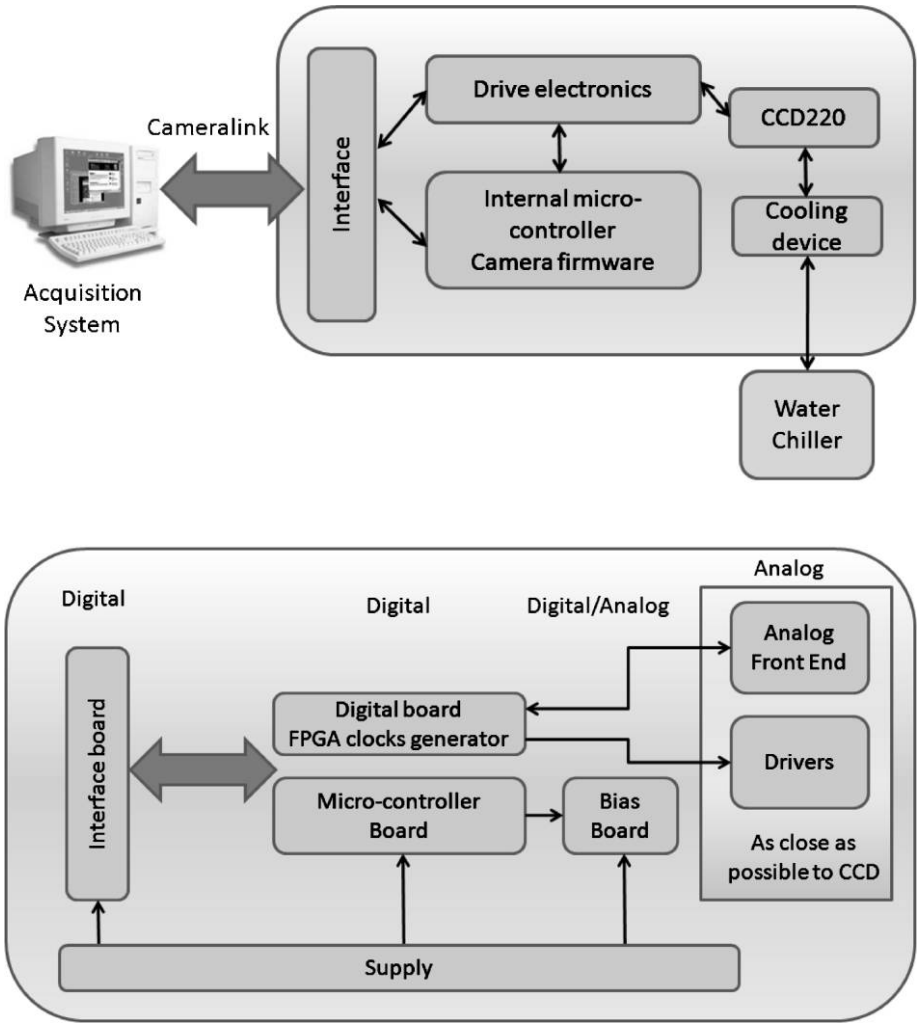

FIG. 5.—OCam controller block diagram. *Top*: OCam controller global architecture. *Bottom*: OCam controller design with detailed breakdown structure of the electronic boards. See the electronic edition of the *PASP* for a color version of this figure.

FIG. 6.—OCam controller views showing the front-end electronics as close as possible to the CCD220. See the electronic edition of the *PASP* for a color version of this figure.

TABLE 1
PULSE AND DC LEVELS USED FOR CCD220 PERFORMANCE MEASUREMENTS

Connection	Description	Pulse amplitude or DC level (V)	Comments
Iφ1,2 high	Image clocks (high)	+3	Rise/fall time <44 ns
Iφ1,2 low	Image clocks (low)	−5	Rise/fall time <44 ns
Sφ1,2 high	Store clocks (high)	+3	Rise/fall time <44 ns
Sφ1,2 low	Store clocks (low)	-5	Rise/fall time <44 ns
Rφ1,2,3 high	Register clocks (high)	+12	Rise/fall time <5.6 ns
Rφ1,2,3 low	Register clocks (low)	0	Rise/fall time <5.6 ns
Rφ2HV high	Multiplication register clock (high) sine wave	+45	Resolution <0.01 V, phase adjustment <1.5 ns, amplitude stability $< \pm 1$ mV, phase stability $< \pm 10$ ps, rise/fall time <100 ns
Rφ2HV low	Multiplication register clock (low)	+4	
φR high	Reset pulse (high)	+10	
φR low	Reset pulse (low)	0	
φC high	DC restore clamp pulse (high)	+10	
φC low	DC restore clamp pulse (low)	0	
RφDC	Multiplication register clock (low)	+3.5	
0G	Output gate	+3	Noise <100 μV rms
OD	Output drain	+28	Noise <25 μV rms
RD	Reset drain	+17	Noise <10 μV rms
SS	Substrate	+3.5	

Thus, the shot-noise curve becomes a straight line when the variance is plotted as a function of the mean signal, and the inverse slope of this linear curve is equal to the system gain in e^- ADU^{-1} (Janesick 2007). This supposes that all other sources of noise are not significant in the acquired data, such as readout noise, photon response nonuniformity noise, or system-correlated noise. It also assumes that no smoothing process such as charge transfer inefficiency has acted to decrease the shot noise, thus invaliding the photon-transfer method. The shot noise has nothing to do with the camera noise and is only due to the nature of light. For this calibration, any mean/variance measurement must be performed without multiplication gain to avoid influence of the excess noise factor from EMCCD devices.

With OCam, we observed that the photon-transfer curve was inappropriate because of correlated noise sources in our system. Finally, the system gain was computed by using the direct measurement of the reset drain current of the whole 240×240 pixel image. The reset drain current is measured with an integrated ammeter embedded inside OCam that measures the total current of each frame with an accuracy of 10 pA. The reset current measured by OCam is simply divided by the frame rate, the number of pixels (240×240), and the charge of the electron to obtain the reset current in e^- pixel^{-1} frame^{-1}. Knowing the reset current in e^- pixel^{-1} frame^{-1} and the mean signal in ADU allows us to plot calibration curves similar to that of Figure 7. This plot is linear; the slope of the linear regression directly gives the mean system gain in e^- ADU^{-1}. This method has the advantage of being valid in any case, with the drawback that the system gain is averaged over the whole frame and cannot be computed separately for each output. A careful calibration of the OCam analog chain gain gives good confidence in the calibration, resulting in a constant system gain over the eight channels of the CCD.

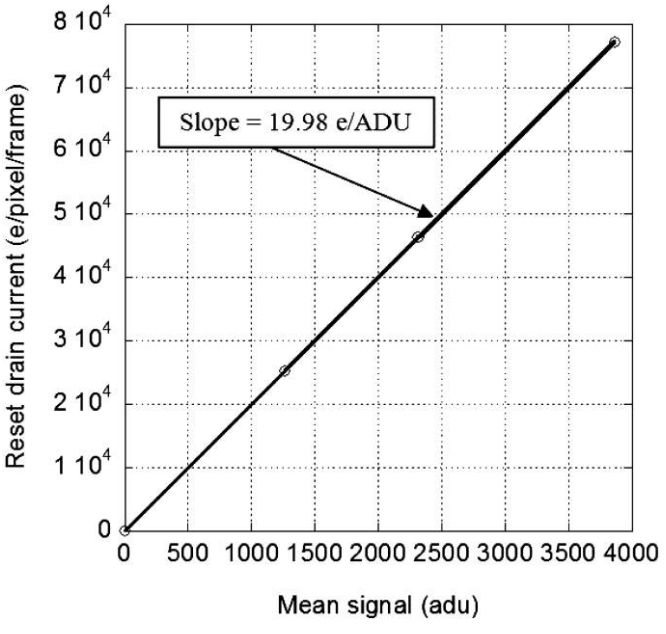

FIG. 7.—Evaluation of the camera average system gain using direct measurement of the reset drain current.

4.2. Method for Measuring Dark Current and Multiplication Gain

Evaluating the multiplication gain and the dark current is not straightforward with an eight-output EMCCD device like the CCD220. A very simple way to evaluate the mean multiplication gain is to use the measurement of the reset drain current. But, again, this is a global method that averages the multiplication gain between the outputs, although it is clear that a certain dispersion of gain is unavoidable with an eight-output EMCCD.

The way dark current and multiplication gain were determined for each output was based on an e2v Technologies technical note (Robbins 2005) for estimating ultralow levels of dark signal in EMCCD devices. If the majority of dark signal is generated in the image/store section, then the dark signal level can be extracted from a simple analysis of the output distribution, even at very low signal levels.

For a certain threshold T of the pixel value, $N_d(T)$ is the fraction of pixels of the distribution that are above the threshold T, G is the multiplication gain, and $S_{\rm dark}$ is the dark signal. $N_d(T)$, T, $S_{\rm dark}$, and G are linked by the following equation (Robbins 2005):

$$Ln(N_d(T)) = Ln(S_{\rm dark}) - T/G.$$

This equation is only valid if the chance of getting two electrons in a pixel is insignificant. If it is not, i.e., if the dark signal is approximately greater than $0.1\ e^-$ pixel^{-1}, then a more complex Monte Carlo analysis must be performed (Robbins 2005). When this equation is valid, the plot of $Ln(N_d(T))$ as a function of the dark signal $S_{\rm dark}$ is linear. Measuring the slope of this linear plot and the intercept with the vertical axis, the dark signal $S_{\rm dark}$ and the multiplication gain G can be computed. Figure 8 shows a typical plot obtained with OCam and the CCD220. The linear part of the plot is fitted in order to derive the dark signal and the multiplication gain. The plot was obtained by combining the 60×120 pixels of an output of 1000 to 2000 consecutive dark images acquired at 1300 fps. This method has been validated by a large number of tests and by cross-comparison with the mean multiplication gain that is measured with the reset drain current ammeter. The method described has the advantage of separately measuring the multiplication gain for each output. The test is performed in complete darkness, thus reducing the possibility of damaging the detector from overillumination while very high multiplication gains are applied.

To compute the noise with multiplication gain on the CCD, a set of 1000 to 2000 consecutive dark images were recorded with multiplication gain of 1000 (~42 V on high-voltage clock). Then for each output, the histogram of all the 60×120 pixels over the cube of images is plotted to ensure good statistics. The mean signal is subtracted to obtain a centered histogram. The rms noise is computed by fitting the histogram with a Gaussian equation:

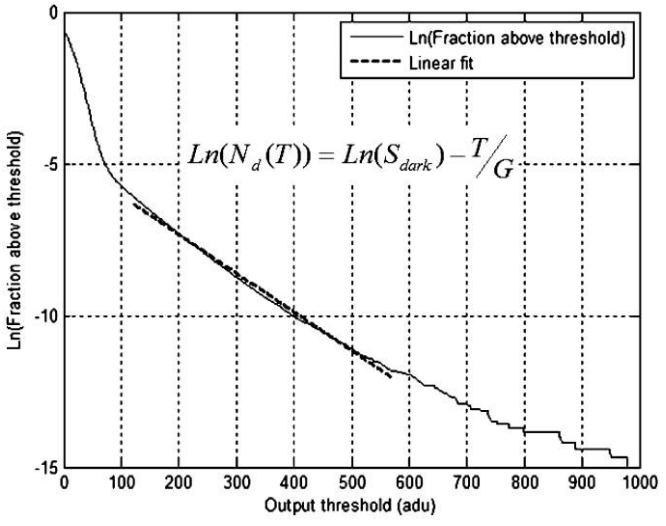

FIG. 8.—Method for computing dark signal and multiplication gain on the EMCCD when the camera is operated with multiplication gain. Statistics are obtained by combining all the pixels of a single output over 1000 to 2000 consecutive frames (60×120 pixels, 1000 dark images). N_d is the fraction of pixels that are above a given threshold T, $S_{\rm dark}$ is the dark signal, and G the multiplication gain. The dark signal and the multiplication gain can be determined by fitting a straight line to the linear part of this figure.

$$N(x) = A \cdot e^{-x^2/2\sigma^2},$$

where σ is the measurement of the camera readout noise (in ADU).

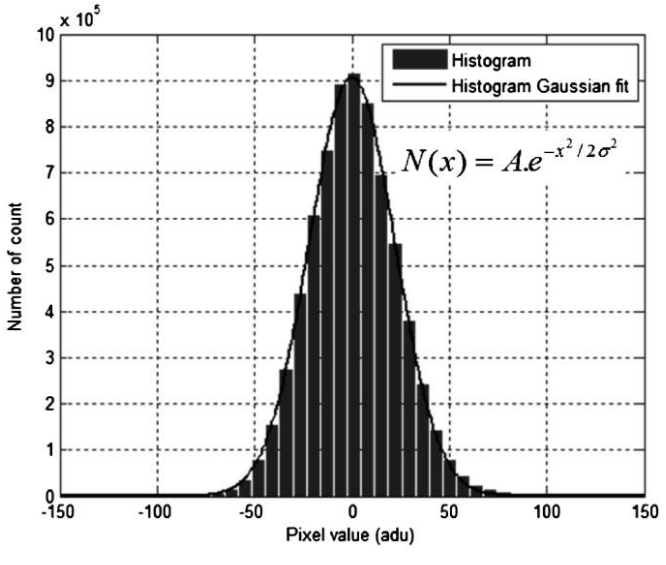

FIG. 9.—Method for computing readout noise with multiplication gain on the EMCCD. The signal is measured here includes the multiplication gain of the EMCCD (multiplication gain is 1560 here). The σ parameter of the histogram Gaussian fit is the rms noise of the camera. See the electronic edition of the *PASP* for a color version of this figure.

TABLE 2
TYPICAL CCD220 AND OCAM MEASURED PERFORMANCES AT 1300 FPS

	HV clock voltage (V)	Multiplication gain	Dark current (e^- pixel^{-1} frame^{-1})	Output noise (e^- rms)	Input-referred noise (e^- rms)	Dark current (e^- frame^{-1})
Amp 0	41.18	915	0.00215	201	0.22	15.5
Amp 1	41.18	905	0.00245	153	0.17	17.7
Amp 2	42.76	880	0.00124	125	0.14	8.9
Amp 3	42.76	954	0.00085	173	0.18	6.1
Amp 4	40.17	1000	0.00009	199	0.20	0.7
Amp 5	40.17	623	0.00144	140	0.22	10.4
Amp 6	42.76	824	0.00038	147	0.18	2.7
Amp 7	42.76	1041	0.00008	180	0.17	0.6
Mean	41.72	893	0.00109	165	0.19	7.8

NOTES.—Measurements taken at 1300 fps with a CCD temperature of -40°C. Subelectron noise at 1300 fps was obtained for the first time. Mean dark signal is ~0.0011 e^- pixel^{-1} frame^{-1}.

Figure 9 shows a typical noise histogram of OCam with multiplication gain (here 1570). Also shown in this figure is the Gaussian fit of the histogram:

From the Gaussian fit of the histogram, the rms readout noise can be derived that is equal to the σ fitted value of the histogram mentioned previously.

4.3. Dark Signal, Multiplication Gain and Noise Measurement

Table 2 shows typical performances of the CCD220 tested with OCam. For the eight outputs (Amplifiers 0–7) of the CCD, the multiplication gain, the dark signal in e^- pixel^{-1} frame^{-1}, the readout noise (using the "spatial" variance method described in Fig. 9) were measured. By multiplying the dark signal by the number of pixels of one output (60×120), the total dark signal per frame (in e^- frame^{-1}) is calculated. The input-referred noise (the readout noise at the input of the multiplication register) is calculated by dividing the output readout noise by the multiplication gain. Measurements presented here were performed at detector temperature of -40°C, a frame rate of 1300 fps, a data cube with 2000 consecutive images, and a mean multiplication gain of 893. Dark current was also measured at 25 fps with multiplication gain. Typical measured results are summarized in Table 3.

The main measured results are as follows:

1. The mean readout noise input-referred is ~0.19 e^- at 1300 fps. The spread in readout noise of the eight outputs is 0.14 e^- to 0.22 e^-, in any case below 0.25 e^-.
2. The mean dark signal is ~0.0011 e^- pixel^{-1} frame^{-1} at 1300 fps, or ~7.8 e^- frame^{-1}.

CCD220 with OCam is currently the only existing system to achieve such low-noise performances at this high readout speed. For the first time, subelectron noise is reported with a frame rate of 1300 fps and a detector format of 240×240 pixels. The total dark signal of ~0.0011 e^- pixel^{-1} frame^{-1} at 1300 fps is also one of the lowest ever reported. This type of measured performance will open up a new era in the field of advanced wavefront sensing. For comparison, the NaCo AO system currently in

TABLE 3
CCD220 AND OCAM MEASURED PERFORMANCE SUMMARY

Test measurement	Result	Unit
Mean readout noise at 1300 fps and multiplication gain ~900	0.2	e^-
Dark signal at 1300 fps at -40°C	<0.01	e^- pixel^{-1} frame^{-1}
Dark signal at 25 fps at -40°C	<0.05	e^- pixel^{-1} frame^{-1}
Detector operating temperature	−40	°C
Peak quantum efficiency at 650 nm	94	%
Linearity at gain x1000 from 10 e^- to 150 e^-	<3	%
Linearity at gain x1 from 15,000 e^- to 150,000 e^-	<3	%
Image area full well capacity at gain x1, 1300 fps	300,000	e^-
Parallel CTE at gain x1, 1300 fps	>0.99995	N/A
Serial CTE at gain x1, 1300 fps	0.99994	N/A
Maximum deviation from peak to valley over the light-sensitive area	0.7	μm
Optical distance from CCD image plane to front of window	3.33	mm
Angle between CCD image plane and front of window	<0.2	°

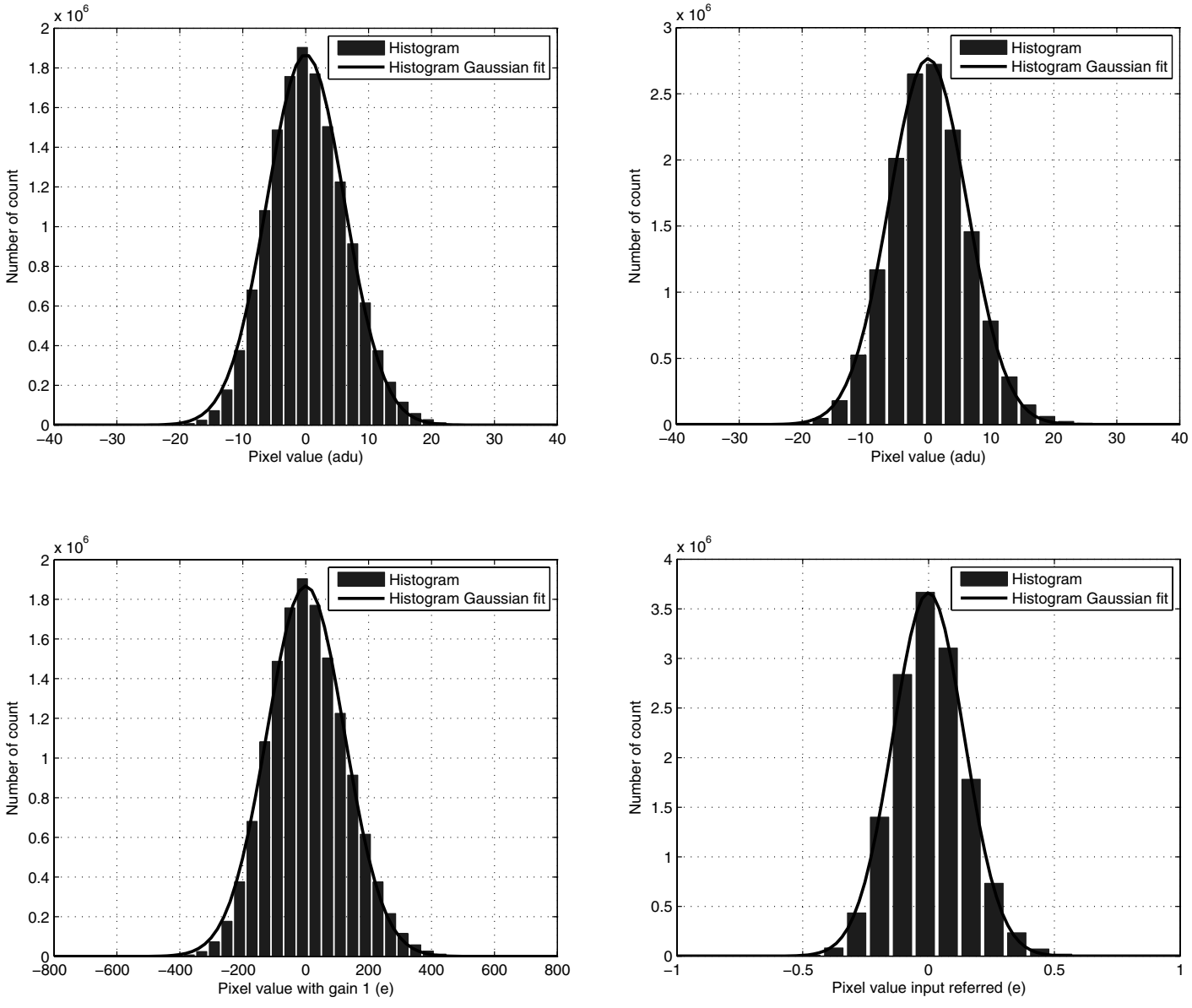

FIG. 10.—Noise histograms of output 2 of CCD220 with OCam. *Top left*: Noise histogram without gain in ADU. *Bottom left*: Noise histogram without gain in e^-. *Top right*: Noise histogram with gain 880 in ADU. *Bottom right*: Noise histogram with gain 880 in e^- and input-referred. Noise as low as 0.14 e^- rms is measured here in these conditions. See the electronic edition of the *PASP* for a color version of this figure.

operation on the ESO VLT uses the CCD50 detector from e2v Technologies and achieves 6–7 e readout noise at 500 Hz frame rate (Feautrier et al. 2000).

Figure 10 illustrates the typical noise behavior of an EMCCD. The left-hand side of the figure shows histograms with a unity gain while the right-hand side of the figure shows histograms measured with multiplication gain. When the signal is multiplied (in this case, by a factor of ~880), the noise histogram remains similar (see the raw data in ADU, in the top part of the figure) but the input-referred noise (in electrons) is dramatically reduced from 123 to 0.14 e^- (see the bottom part of the figure). Figure 11 shows the mean noise of the eight CCD outputs input-referred as a function of the multiplication gain.

4.4. Quantum Efficiency

The quantum efficiency (QE) of the detector is also a major parameter of the system sensitivity. The QE of the standard silicon CCD220 was measured, and typical results are shown in Figure 12 using the calibration parameters of the previous section (i.e., a system gain of 20 e^- ADU^{-1}). Also shown in this figure with square symbols is the specified QE. It shows

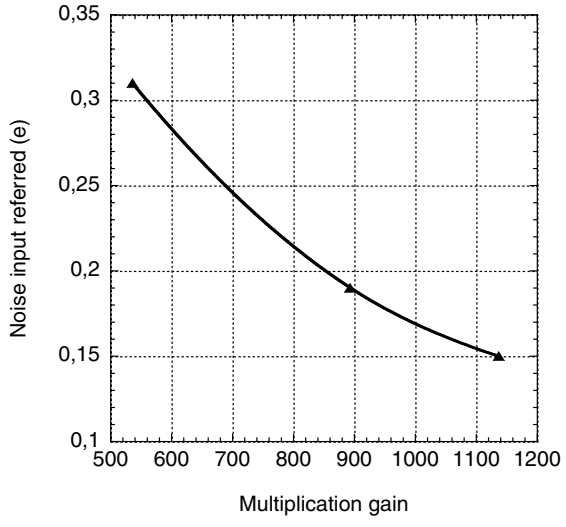

FIG. 11.—Mean noise of the eight CCD outputs input-referred as a function of the multiplication gain.

that the measured QE exceeds the specified value at all wavelengths and peaks at 94% at a wavelength of 650 nm.

4.5. CCD220 and OCam Performance Measurement Summary

Many other features of the CCD220 were tested with conventional methods that are not described here. These performances are summarized in Table 3. A first set of four electrical grades, four engineering grades, and four science grades devices were delivered as part of the original ESO/OPTICON contract in 2009. Since this milestone, production runs have started at e2v Technologies to routinely deliver CCD220 to other customers.

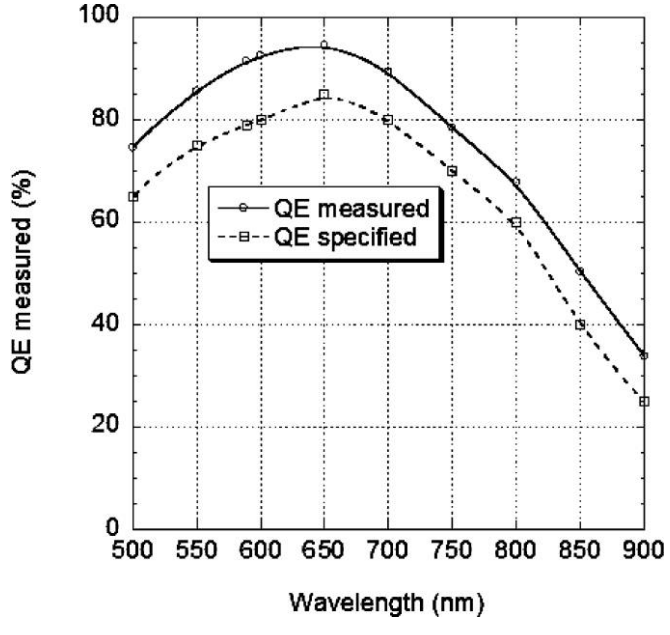

FIG. 12.—CCD220 measured QE of standard silicon variant compared with the specified values (square symbols).

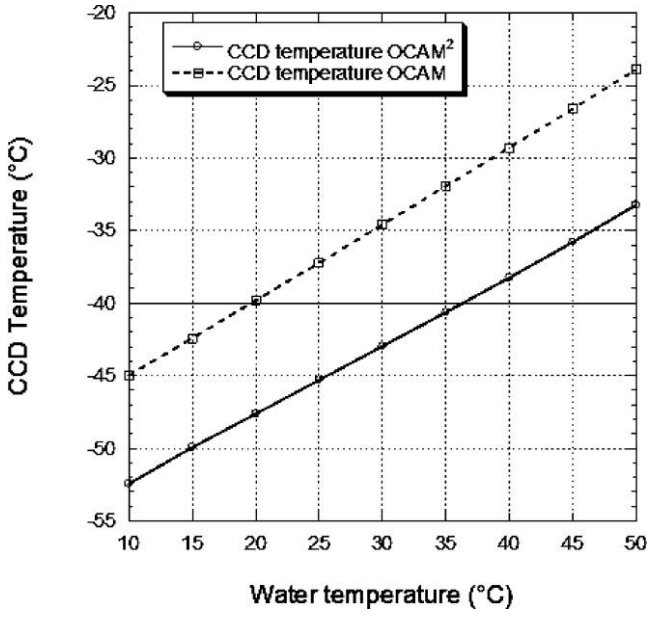

FIG. 13.—CCD temperature as a function of water temperature (flow of 1.5 liters minute^{-1}) used in the heat sink dedicated to cool the Peltier hot side with outside air temperature of 30°C. As shown in this figure, OCam can accommodate a water temperature as high as +40°C with a CCD temperature close to −40°C in these rugged conditions.

5. ADVANCING FROM OCAM TO OCam^2

OCam^2 is the production version of OCam commercialized by First Light Imaging.[8] Whereas OCam has been designed to test CCDs and provides many tuning capabilities (voltages, features, and so on), OCam^2 is a ready-to-use camera with embedded parameters to run the CCD factory-optimized. OCam^2 has also been designed for ruggedness and can cope with more demanding environmental conditions, like accepting cooling water temperature up to 35°C and removing the need for an external chiller (see Fig. 13). The camera is fully sealed, includes the thermoelectric cooler controller inside the camera head, and needs only a standard +24 V power supply for the whole system. A photograph of OCam^2 is shown in Figure 14.

OCam^2 uses high-performance field-programmable gate arrays and can perform instant on-the-fly preprocessing like dark/bias subtraction and flat-gain correction, lowering the computing power required by the real-time computer. OCam^2 provides not only an industry-standard CameraLink full interface, but also duplex serial protocols over multimode or monomode fiber optics using standard small form-factor pluggable modules.

[8] See http://www.firstlight.fr/.

FIG. 14.—Photograph of OCam^2: the OCam production camera commercialized by First Light Imaging. *Left*: Camera black aluminum cover. *Right*: Inside of the camera, where the CCD220, all the electronic boards, and the water heat exchanger can be seen.

Protocols like PCI Express, RapidIO, and Infiniband are supported. Other specific, or even proprietary, fiber links can be implemented upon request. Unique external synchronization and clock inputs of OCam^2 ensure a perfect synchronous operation of any number of OCam^2 cameras at the nanosecond level. It is possible to synchronize OCam^2 with any external device (pulsed laser, another OCam^2 camera, or master timer) with a precision of 10 ns. OCam^2 also includes a modified mechanical design allowing the integration of any type of microlens array. This allows the use of this camera in all kinds of wavefront-sensing AO applications. The front cover of OCam^2 can be easily modified to include a microlens exchange mechanism. Custom microlens array integration can easily be performed based on a flexible mechanical design of the front cover and past experience of microlens integration in the most advanced existing AO systems. The size of the camera head is extremely compact, with a $238.5 \times 175 \times 76.2$ mm footprint that includes all electronics, the CCD, and the cooling system embedded in a robust aluminum sealed cover. The services needed to operate the camera are not demanding. OCam^2 only needs a 24 V DC power supply and a water cooling system with the following typical specifications: a water flow of 1.5 liters minute^{-1}, a cooling power of 50 W, and water temperature between 10 and 35°C.

With the capability of running at 2500 fps by using optimized clocking, a special preamplifier design that rejects clock feedthrough, and many other features, Ocam^2 makes it an interesting contender for AO applications of the planned generation of extremely large telescopes.

6. CONCLUSION

For the first time, the CCD220 and OCam have demonstrated subelectron noise for a 240×240 pixel camera system running at 1300 fps, with the detector operated at a temperature of -40°C. This article reports on the performance characterization of OCam and the CCD220; this includes readout noise, dark current, multiplication gain, quantum efficiency, and charge transfer efficiency. The CCD220 is a new detector fabricated by e2v Technologies based on their L3Vision technology. It includes eight outputs, split frame-transfer architecture to lower detector smearing while the detector is read, eight L3Vision registers to have multiplication gain, and subelectron noise at high speed. Both developed within the European OPTICON network, the CCD220 detector and the OCam camera were designed for AO applications with optimized performances in terms of noise and frame rate. A deep depleted variant of the CCD220 also exists with the same overall performances and improved QE at red wavelengths.

A world record of $0.19\ e^-$ mean rms Noise was achieved with the 240×240 pixel CCD220 at 1300 fps and a multiplication gain of 900. Under these conditions, the mean dark current is close to $0.001\ e^-$ pixel^{-1} frame^{-1}, and the peak QE is 94% at 650 nm wavelength, due to back-thinning and back-illumination of the CCD. This achievement is a major breakthrough in the field of wavefront sensing for advanced adaptive optics systems. This new technological development will be used in the next generation of ground-based telescope instruments. It will strongly impact the performance of the most advanced AO systems to be developed for future instruments.

A production camera called OCam^2 and based on OCam experience is designed and commercialized to run at 1500 fps without degrading OCam performances. OCam^2 has been designed for ruggedness and can accept more demanding environmental conditions. The OCam^2 detector is fully cooled by three Peltier stages in order to avoid complex and costly cryogenic systems. Another advantage of this design is the extreme compactness of the camera head, embedding all the electronics (analog, digital, and Peltier drivers) and making it easy to integrate into a multi-wavefront-sensing AO system with an extremely small footprint. Ready to use, OCam^2 is designed for reliable operation on a telescope. A future development will start soon to speed up the frame rate of OCam^2 to 2500 Hz in order to accommodate the most demanding extreme AO applications that will come in the future.

REFERENCES

Beuzit, J., Feldt, M., Dohlen, K., Mouillet, D., Puget, P., Wildi, F., Abe, L., Antichi, J., et al. 2008 Proc. SPIE, 7014, 701418

Downing, M., Arsenault, R., Baade, D., Balard, P., Bell, R., Burt, D., Denney, S., Feautrier, P., et al. 2006, Proc. SPIE, 6276, 62760H

Downing, M., Finger, G., Baade, D., Hubin, N., Iwert, O., & Kolb, J. 2008, Proc. SPIE, 7015, 70151R

Downing, M., Hubin, N., Kasper, M., Jorden, P., Pool, P., Denney, S., Suske, W., Burt, D., et al. 2006, in Scientific Detectors for

Astronomy 2005 ed. J. E. Beletic, J. W., Beletic, & P., Amico (Dordrecht: Springer), 336, 321
Feautrier, P., Fusco, T., Downing, M., Hubin, N., Gach, J-L., Balard, P., Guillaume, C., Stadler, E., et al. 2006, in Scientific Detectors for Astronomy 2005, ed. Jenna E., Beletic, Beletic, James W., & Paola, Amico (Dordrecht?: Springer), 336, 315
Feautrier, P., Gach, J., Balard, P., Guillaume, C., Downing, M., Stadler, E., Magnard, Y., Denney, S., et al. 2008, Proc. SPIE, 7021, 70210C
Feautrier, P., Kern, P. Y., Dorn, R. J., Rousset, G., Rabou, P., Laurent, S., Lizon, J., Stadler, E., et al. 2000, Proc. SPIE, 4007, 396
Feautrier, P., Stadler, E., Downing, M., Hurrell, S., Wheeler, P., Gach, J., Magnard, Y., Balard, P., et al. 2006, Proc. SPIE, , 6271, 62710S
Fusco, T., Nicolle, M., Rousset, G., Michau, V., Beuzit, J-L., & Mouillet, D. 2004, Proc. SPIE5490, 1155
Gach, J-L., Balard, P., Boissin, O., Downing, M., Feautrier, P., Guillaume, C., & Stadler, E. 2006, in Scientific Detectors for Astronomy 2005, ed. J. E. Beletic, J. W. Beletic, & P., Amico (Dordrecht: Springer), 336, 639
Gillmore, G. F. 2004, Proc. SPIE, 5382, 138
Janesick, J. 2007, Photon Transfer (PM170; Bellingham: SPIE)
Jerram, P., Pool, P. J., Bell, R., Burt, D. J., Bowring, S., Spencer, S., Hazelwood, M., Moody, I., et al. 2001, "Proc. SPIE, 4306, 178
Moorwood, A. 2006, Proc. SPIE, 6269, 626904
Petit, C., Fusco, T., Charton, J., Mouillet, D., Rabou, P., Buey, T., Rousset, G., Sauvage, J.-F., et al. 2008, Proc. SPIE, 7015, 70151D
Reyes, J., & Conzelman, R. 2009, Poster at Detectors for Astronomy 2009 (12-B; Garching: ESO)
Robbins, M. 2005, Estimating Ultra Low Levels of Dark Signal Using an L3Vision Device (L3V-TN-635; Chelmsford: e2v Technologies)
Robbins, M., & Hadven, B. 2003, IEEE Trans. Electron Devices, 50, 1227